Geophysical Research Letters

Key Points:
- The low single scattering albedo in biomass burning aerosol (BBA) over southern West Africa results from the presence of refractory black carbon
- The brown carbon contribution to the aerosol absorption is negligible in these well-aged BBA plumes
- Accounting for the diversity in black carbon mixing state is needed to accurately estimate BBA optical properties

Supporting Information:
- Supporting Information S1

Correspondence to:
C. Denjean,
cyrielle.denjean@meteo.fr

Unexpected Biomass Burning Aerosol Absorption Enhancement Explained by Black Carbon Mixing State

Cyrielle Denjean[1], Joel Brito[2,3], Quentin Libois[1], Marc Mallet[1], Thierry Bourrianne[1], Frederic Burnet[1], Régis Dupuy[2], Cyrille Flamant[4], and Peter Knippertz[5]

[1]CNRM, Université de Toulouse, Météo-France, CNRS, Toulouse, France, [2]LaMP, Université de Clermont Auvergne, Clermont-Ferrand, France, [3]IMT Lille Douai, Université de Lille, SAGE, Lille, France, [4]LATMOS/IPSL, Sorbonne Université, UVSQ, CNRS, Paris, France, [5]Institute of Meteorology and Climate Research, Karlsruhe Institute of Technology, Karlsruhe, Germany

Abstract Direct and semi-direct radiative effects of biomass burning aerosols (BBA) from southern and central African fires are still widely debated, in particular because climate models have been unsuccessful in reproducing the low single scattering albedo in BBA over the eastern Atlantic Ocean. Using state-of-the-art airborne in situ measurements and Mie scattering simulations, we demonstrate that low single scattering albedo in well-aged BBA plumes over southern West Africa results from the presence of strongly absorbing refractory black carbon (rBC), whereas the brown carbon contribution to the BBA absorption is negligible. Coatings enhance light absorption by rBC-containing particles by up to 210%. Our results show that accounting for the diversity in black carbon mixing state by combining internal and external configurations is needed to accurately estimate the optical properties and henceforth the shortwave direct radiative effect and heating rate of BBA over southern West Africa.

Plain Language Summary Extensive seasonal fires over southern and central Africa result in the transport of massive amounts of biomass burning aerosols over huge areas of the eastern Atlantic Ocean. Recent field observations highlight that biomass burning aerosols transported from the coast of southern Africa to the far north over southern West Africa were characterized by low single scattering albedo. This finding is of paramount interest, because radiative heating within the absorbing aerosol layer is hypothesized to affect the low cloud deck over this specific region and may ultimately influence the large-scale circulation. However, debate remains about the causes of the low single scattering albedo by biomass burning aerosols, causing ambiguous parameterizations of their optical properties in climate models. Here we present simultaneous airborne measurements of the composition and optical properties of biomass burning aerosols transported over southern West Africa. We show that black carbon particles dominated the light absorption by biomass burning aerosols at mid-visible wavelengths. Our findings indicate that the black carbon mixing state plays a significant role in the aerosol optical properties and may be an important modulator to be considered in climate models for simulating direct and semi-direct radiative effects of biomass burning aerosol over southern West Africa.

1. Introduction

Biomass burning aerosols (BBAs) are an important component of the climate system due to their strong absorption of solar radiation and the associated impact on the atmospheric energy budget and cloud fraction (i.e., direct and semi-direct aerosol radiative effects, DRE and SDE) (Myhre, Shindell, et al., 2013; Wilcox, 2012). Extensive seasonal fires result in the transport of massive amounts of BBA from southern and central Africa over huge areas of the eastern Atlantic Ocean (Haslett et al., 2019; Menut et al., 2018; Zuidema et al., 2018), which constitutes the Earth's region with the largest aerosol optical depths above clouds (Peers et al., 2016; Waquet et al., 2013). Over this specific region, shortwave heating within the absorbing aerosol layer is hypothesized to affect the low cloud deck through modification of the atmospheric stability (Adebiyi & Zuidema, 2016; Herbert et al., 2020; Sakaeda et al., 2011; Wilcox, 2010) and may ultimately influence the large-scale circulation (Randles & Ramaswamy, 2010). A number of field campaigns—including Dynamics-Aerosol-Chemistry-Clouds Interactions in West Africa (DACCIWA),

Aerosols, Radiation and Clouds in southern Africa (AEROCLO-sA), Layered Atlantic Smoke Interactions with Clouds (LASIC), ObseRvations of Aerosols above CLouds and their intEractionS (ORACLES), and Cloud and Aerosols Radiative Impact and Forcing (CLARIFY)—have recently been carried out over the eastern Atlantic Ocean, with the aim to better quantify the BBA radiative effects (Flamant, Knippertz, et al., 2018; Formenti et al., 2019; Zuidema et al., 2016, 2018). Both in situ and remote-sensing observations acquired during these campaigns have all emphasized a strong shortwave (SW) absorption (low single scattering albedo, SSA) in BBA transported from the coast of southern Africa to the far north over southern West Africa (SWA) (Chylek et al., 2019; Denjean et al., 2020; Pistone et al., 2019; Wu et al., 2020; Zuidema et al., 2018). This means that BBA over this climatically important region is more absorbing than is currently represented in climate models (Mallet et al., 2019; Peers et al., 2016; Stier et al., 2013). However, debate remains about the causes of this low SSA in these BBA plumes.

The absorption of sunlight by BBA particles is largely driven by refractory black carbon (rBC) (Bond et al., 2004). Coating of rBC-containing particles with light scattering material can enhance the absorption of the rBC core due to the so-called "lensing effect" and can thus amplify their impact (Bond et al., 2013). Absorption enhancement (E_{abs}) is defined as the absorption by mixed rBC-containing particles relative to absorption by the same amount of rBC in pure, uncoated particles. Currently, there are only few—and partly contradictory—studies reporting E_{abs} of ambient BBA. Negligible enhancements ($E_{abs} \sim 1$) have been reported in BBA originating from forest fires in North America, even when substantial coatings were present (Cappa et al., 2012; Healy et al., 2015), whereas E_{abs} values up to 1.6 have been observed in the Amazonia region (Lack et al., 2012; Liu et al., 2017). Several hypotheses have been put forward to explain this variability: (1) A restructuring of rBC-containing particles from fractal morphologies towards a compact core could counteract the lensing effect (Kahnert & Kanngießer, 2020; Shingler et al., 2016); (2) rBC-containing particles are not entirely coated but instead exhibit an aggregate structure with non-rBC material (Liu & Mishchenko, 2007), thus leading to overall little change in absorption by rBC-containing particles when internally mixed (Wu et al., 2018); (3) BBA absorption enhancement is partly attributed to the presence of light-absorbing organic aerosols termed brown carbon (BrC) (Brown et al., 2018; Chylek et al., 2019); (4) accounting for mixing-state diversity within the rBC-containing particle population (i.e., the distribution of coating material across the ensemble of rBC-containing particles), as has been done by Fierce et al. (2016) and Liu et al. (2017), is necessary to accurately quantify the average absorption. In part because of the paucity of comprehensive ambient measurements of rBC mixing state in BBA plumes, the mechanisms responsible for the large variation of E_{abs} remain elusive. In addition, previous studies lacked assessing the effect of rBC mixing state on the SSA, which is a key parameter for the quantification of DRE and SDE. As a result, the representation of BBA optical properties in current climate models is uncertain, and many models assume that all rBC-containing particles are externally mixed (Chung et al., 2012; Myhre, Samset, et al., 2013) or use a constant E_{abs} (typically 1.5 as recommended in Bond & Bergstrom, 2006) to account for coating by other species. Here we use airborne in situ measurements to demonstrate how the rBC mixing state impacts key-climate relevant optical properties in BBA plumes. Our results highlight that the mixing state of rBC-containing particles may be an important modulator to be considered in climate models for simulating BBA absorbing properties, DRE and SDE over the eastern Atlantic Ocean.

2. Methods

2.1. Biomass Burning Source and Transport to SWA

As part of the DACCIWA project (Knippertz et al., 2015), the ATR-42 airborne platform of SAFIRE performed 20 flights over the Gulf of Guinea and inland from 29 June to 16 July 2016 (Flamant, Knippertz, et al., 2018). Aerosol and trace gas measurements revealed two distinct BBA layers over SWA (Denjean et al., 2020; Flamant, Knippertz, et al., 2018; Haslett et al., 2019), namely, (i) a lower layer located in the marine boundary layer (BL-BBA) and (ii) an upper, about 2 km-thick layer centered at ~3 km above sea level (FT-BBA). In the DACCIWA region, the widespread low level clouds commonly lead to a decoupled BL which top is located at about 500 m above sea level deep away from the coast and about 800 m at the coast (Flamant, Deroubaix, et al., 2018). Denjean et al. (2020) examined measurements of BBA size distribution and optical properties from straight level runs (SLRs) and vertical profiles. Here

we use the same 13 SLRs measurements as in Denjean et al. (2020). Supporting information Figure S1 and Table S1 summarize the geographical location, date, time, and altitude of these 13 SLRs.

The source locations of BBA have been analyzed using the chemistry-transport models CHIMERE, COSMO-ART, GEOS-Chem, and WRF (Flamant, Knippertz, et al., 2018; Haslett et al., 2019; Menut et al., 2018). The results indicate that all BBA originated from fires in the tropical and subtropical grasslands, savannas, and scrubland areas of southern and central Africa. Additional assessments using the backward trajectories from the HYSPLIT model in conjunction with the fire spot data from the MODIS satellite confirm this origin, as shown in Figure S1. The BBA plumes were sampled by the aircraft after estimated aging larger than 1 week.

2.2. Aircraft Instrumentation and Data Analysis

The aircraft was extensively equipped to measure gas and aerosol properties. Onboard aerosol instruments sampled ambient air via stainless steel tubes through the Community Aerosol Inlet (CAI). This is an isokinetic and isoaxial inlet with a 50% sampling efficiency for particles with a diameter of 5 μm (Denjean et al., 2016).

Here, we use in situ data obtained using a single-particle soot photometer (SP2). The SP2 measures the mass of rBC within single aerosol particles in the size range of 70–600 nm based on laser-induced incandescence. The mass equivalent diameter of rBC cores ($D_{core\ rBC}$) was derived from the mass of rBC per particle assuming the density of rBC as 1.8 g cm^{-3} based on the recommendations of Bond and Bergstrom (2006). SP2 data were also used to estimate the optical diameter of rBC-containing particles ($D_{total\ rBC}$), using a slightly modified version of the leading-edge-only method described by Gao et al. (2007) as implemented *by* Laborde et al. (2012). A detailed description of this method, including a description of the SP2 calibration and the method used for data quality control, is shown in section S1. The rBC mixing state of each particle can be expressed as a mass mixing ratio, that is, the mass of non-rBC material in a rBC-containing particle divided by the mass of rBC. The bulk mass mixing ratio ($M_{R,bulk}$) for a given time window is then calculated as follows:

$$M_{R,\ bulk} = \left(\frac{\sum_i D_{total\ rBC,\ i}^3}{\sum_i D_{core\ rBC,\ i}^3} - 1 \right) \times \frac{\rho_{coating}}{\rho_{rBC}}$$

where $\rho_{coating}$ is the coating density assumed to be 1.5 g cm^{-3}.

The aerosol chemical composition for non-refractive compounds was measured using an Aerodyne compact Time-of-Flight Aerosol Mass Spectrometer (HR-ToF-AMS). For a more detailed description of the instrument and data analysis, the reader is referred to Brito et al. (2018). The aerosol number size distribution was measured with a custom-built scanning mobility sizer spectrometer (SMPS, 20–485 nm), an ultra-high sensitivity aerosol spectrometer (UHSAS, 0.04–1 μm), and an optical particle counter (OPC GRIMM model 1.109, 0.3–32 μm). The aerosol absorption coefficient (σ_{abs}) was measured using a three-wavelength particle soot absorption photometer (PSAP) with an uncertainty of 8% (Davies et al., 2019). The PSAP measures changes of filter attenuation due to the collection of aerosol deposited on the filter, which were corrected for the scattering artifacts according to the Virkkula (2010) method. The particle scattering coefficient (σ_{scat}) was measured using a TSI 3563 3-Wavelength Integrating Nephelometer and corrected for angular truncation error by using Lorenz-Mie scattering model, number size distributions, and the complex refractive index provided in Denjean et al. (2020) for the same sampled BBA. Uncertainty in σ_{scat} measured with the nephelometer is estimated to be 5% (Muller et al., 2011). The concentration of carbon monoxide (CO) was measured with an ultraviolet and infrared analyzer (Picarro).

The mass absorption cross section of rBC (MAC_{rBC}) and the enhancement factor of light absorption of rBC due to the lensing effect (E_{abs}) are defined, respectively, as follows:

$$MAC_{rBC}(\lambda) = \frac{\sigma_{abs(\lambda)}}{M_{rBC}}$$

and

$$E_{abs}(\lambda) = \frac{MAC_{rBC}(\lambda)}{MAC_{uncoated\ rBC}(\lambda)}$$

where λ is the wavelength. The uncertainty in MAC_{rBC} and E_{abs} is ±12% by propagating the uncertainties of M_{rBC} and σ_{abs}. The reference $MAC_{uncoated\ rBC}$ is determined by extrapolating the observed relationship

between coating thicknesses ($M_{R,bulk}$) and MAC_{rBC} to the limit of no coating material (Figure S2). The resulting $MAC_{uncoated\ rBC}$ value for BBA during DACCIWA is 7.7 m^2 g^{-1} at 550 nm. This value agrees with the value of 7.5 $\pm$ 1.2 m^2 g^{-1} reported in the review of Bond and Bergstrom (2006).

The absorption Angstrom exponent (AAE), which describes the wavelength dependence of aerosol absorption, is calculated between 450 and 660 nm as follows.

$$AAE = -\frac{\ln\left(\frac{\sigma_{abs}(450)}{\sigma_{abs}(660)}\right)}{\ln\left(\frac{450}{660}\right)}$$

The uncertainty in AAE is estimated to be 5% (Davies et al., 2019).

The SSA and asymmetry factor (g) are defined respectively as follows:

$$SSA = \frac{\sigma_{scat}(\lambda)}{\sigma_{scat}(\lambda) + \sigma_{|abs|(\lambda)}}$$

and

$$g(\lambda) = \frac{1}{2}\int_0^\pi cos(\theta)sin(\theta)P(\theta,\lambda)d(\theta)$$

with $P(\theta,\lambda)$ the scattering phase function and θ the scattering angle. g was calculated using Lorenz-Mie scattering model and measured size distribution (Denjean et al., 2020). The uncertainties in SSA and g are estimated to be 9% and 13%, respectively, by propagating the uncertainties of σ_{scat} and σ_{abs}.

The aerosol properties were measured at dry conditions (RH < 30%). Data obtained in clouds were excluded from analysis to avoid inlet artifacts. Aerosol data are reported at standard temperature and pressure conditions (273.15 K and 1013.25 hPa).

2.3. Modeling BBA Optical and Radiative Properties
2.3.1. Lorenz-Mie Scattering Calculations
The influence of observed coatings of rBC-containing particles on BBA optical properties relevant to parameterizing aerosol radiative effects in models (MAC, SSA, and g) was investigated using a Lorenz-Mie scattering model with the core-shell assumption (Bohren & Huffman, 1983). The rBC-containing particles are assumed to have concentric-sphere morphology with a spherical rBC core embedded in a shell of internally mixed nonabsorbing material. The use of Mie theory, which assumes that the particles are spherical, is supported by the overall range of AAE (see section 3.2) that is typical for rBC particles in a core–shell morphology, whereas much larger AAE would be expected for more complex morphologies (Liu & Mishchenko, 2007). The calculations were performed at the wavelength of 550 nm for each BBA plume using observations, namely, the size distributions of rBC-containing and rBC-free particles and the mass fraction of rBC-containing particles in the aerosol population (f_{rBC}). The size distribution of rBC-free particles was derived by substracting the SP2-measured size distribution of rBC-containing particles (which includes both coated and noncoated particles) from the total aerosol size distribution measured using the SMPS, UHSAS, and OPC GRIMM. The refractive index of the rBC core at the wavelength of 550 nm was assumed to be 1.95–0.79i (Bond & Bergstrom, 2006). Because the analysis of aerosol chemical composition indicates the predominance of organic and sulfate species in BBA (see section 3.1), the refractive index of the coating material and BC-free particles was assumed to be 1.50-0i (Fuller et al., 1999). Densities of 1.8, 1.2, and 1.7 g cm^{-3} were used for rBC, organics, and inorganics, respectively, for the conversion of mass fractions to volume fraction.

2.3.2. ecRaD Radiative Transfer Model
The offline version of the radiative code ecRad (Hogan & Bozzo, 2018), operationally used at the European Center for Medium-Range Weather Forecasts (ECMWF), was used to compute the SW radiative forcing of BBA in clear-sky and cloudy-sky conditions. To this end, an average atmospheric profile was built from the airborne measurements taken during the campaign, including vertical profiles of pressure, temperature,
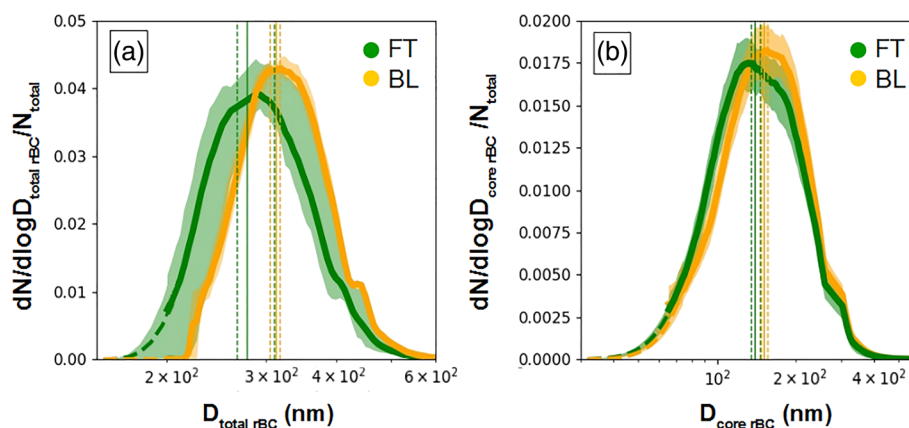
Figure 1. Number size distributions normalized by the total number concentration of (a) coated rBC particles and (b) rBC cores. The dashed lines are Gaussian distributions fitted to the mass distribution and converted to the corresponding number distributions. Colored areas represent the 25th and 75th percentiles of the number size distributions. The vertical bars show the median values (solid lines) and the 25th and 75th percentiles (dashed lines) of the geometric diameter for the two BBA categories.

relative humidity, and CO_2. Vertical distributions of BBA mass concentration measured in situ during vertical profiles (Denjean et al., 2020) were averaged over the campaign and used as input in ecRaD (Figure S2). BBA optical properties (*MEC*, *SSA*, and *g*) at 550 nm were constrained either from our observations (Denjean et al., 2020) or from the three optical models presented in section 2.3.1. These input parameters were extended to the full SW spectrum assuming the same spectral variations as the rBC natively implemented in ecRad. The SW DRE at the top of the atmosphere (TOA) and atmospheric heating rates due to BBA were computed as the difference between simulations including aerosols and reference aerosol-free simulations. The simulations were performed assuming a surface albedo of 0.25, typical of the rainforest above which the measurements were taken (Moody et al., 2005). The cosine of the solar zenith angle was set to 0.8, which corresponds to the weighted daily average value during the campaign. The simulations conducted under cloudy-sky conditions assumed a cloud optical thickness of 10 located at 2.4 km, at the top of the boundary layer (2.4 km). The cloud optical properties were computed according to the parameterization of Edwards and Slingo (1996). To this end, the cloud droplet effective radius was assumed to be 5 μm, which is consistent with the observations by Taylor et al. (2019) during DACCIWA.

3. Results

3.1. rBC Mixing State

Figure 1 shows size distributions of rBC-containing particles (panel A) and rBC cores only (panel B) for the boundary layer (BL) and free troposphere (FT). The modal $D_{total\ rBC}$ decreases from ~310 in the BL to ~280 nm in the FT. This is mainly attributed to the increasing coating thickness in BL-BBA, since the geometric diameters of rBC cores are ~140 and ~152 nm, respectively. The coating thicknesses translate into an average $M_{R,bulk}$ of ~4.7 and ~ 6.0 in FT-BBA and BL-BBA, respectively. This indicates that rBC-containing particles were mostly constituted of non-rBC materials, making up more than four times the rBC mass in these rBC-containing particles. In addition, the percentage of coated rBC particles and the average coating thicknesses, respectively, as observed in the BL (91% and 159 nm), are larger than those measured in the FT (88% and 137 nm).

The variability of rBC coating thickness could result either from differences in the sources or from aging processes affecting BBA plumes during the long-range transport of BBA over SWA. We have compared the correlation between M_{rBC} and ΔCO (ΔCO = plume CO – background CO) to gain information about the BBA sources (Spackman et al., 2008). In addition, the M_{rBC} to ΔCO ratio is useful for evaluating the potential influence of wet removal processes on BBA, as precipitation scavenging affects rBC-containing particles but does not affect CO (Moteki et al., 2012; Taylor et al., 2014). The background value of CO was
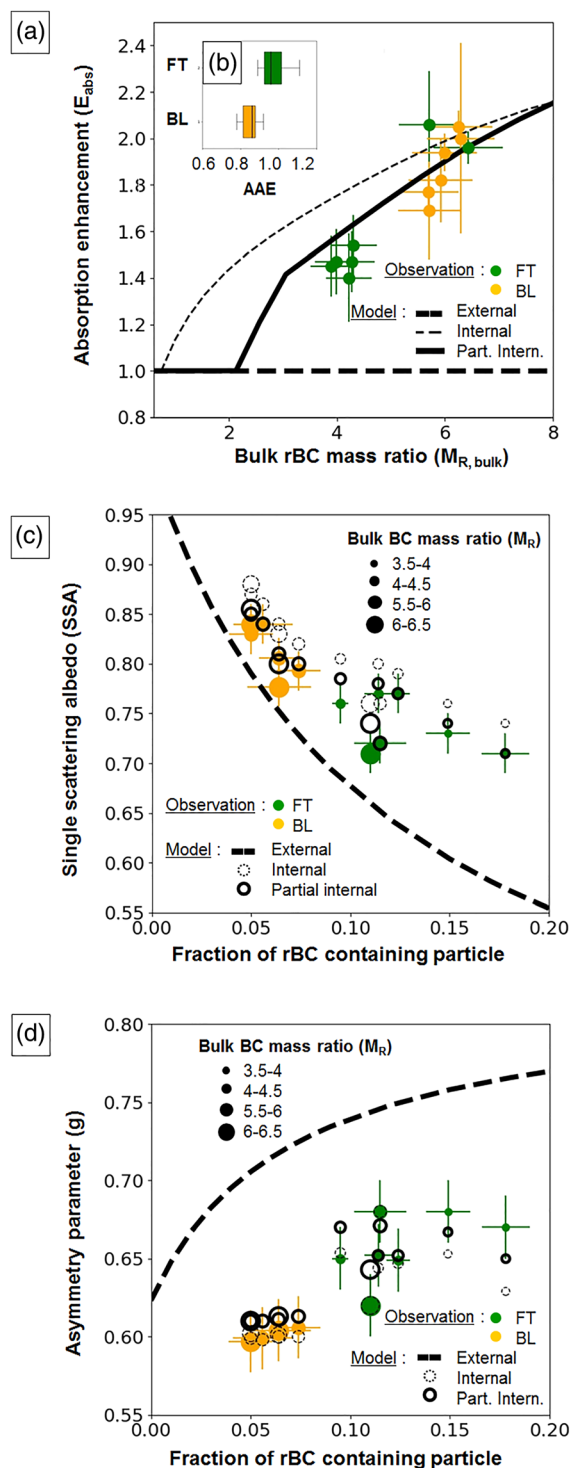
Figure 2. Sensitivity of BBA optical properties to rBC mixing state. Measured and modeled employing different rBC population mixing state (external, internal, and partial internal) of (a) absorption enhancement at 550 nm as a function of $M_{R,bulk}$, (b) Angtrom absorption exponent calculated between 450 and 660 nm, (c) single scattering albedo at 550 nm as a function of fraction of rBC containing particle in the total aerosol mass, and (d) asymmetry parameter at 550 nm as a function of mass fraction of rBC-containing particles in the total aerosol mass. Error bars are one standard deviation over the mean.

estimated with the intercept of rBC versus CO using all data points available within the plume. It ranged from 80 to 95 ppb depending on the altitude of the BBA plume. The correlations between M_{rBC} and ΔCO were similar for BL-BBA and FT-BBA (Figure S4), with mean values of the M_{rBC} to ΔCO ratio of 7.4 and 7.6 ng m^{-3} ppb^{-1}, respectively. These values are comparable to those previously reported in BBA from southern and central African fires near emission sources (7.4 ng m^{-3} ppb^{-1} in the review of Andreae & Merlet, 2001) and SWA (7.4 ng m^{-3} ppb^{-1} by Capes et al., 2008). This suggests that BBA-BL and BBA-FT in the present work had similar source locations and had not been influenced by wet removal processes during transport.

Measurements of the aerosol composition during DACCIWA revealed a larger contribution of sulfate in BL-BBA (~27%) (Figure S5), which was traced back to a strong influence of marine emissions (Haslett et al., 2019). In addition, given the large loadings of organic aerosol in BBA over SWA (greater than 50%), we expect organic aerosol to contribute significantly to the coating over rBC cores. The organic aerosol within BBA plumes over SWA was highly oxidized, being dominated by a peak at m/z 44 and with low contribution of m/z 60 towards the total organic aerosol mass (Figure S6), as discussed in Haslett et al. (2019). Although both BBA layers were found to be highly oxidized, the f_{44}/f_{43} (the fraction of the organic aerosol mass spectrum signal at m/z 44 and 43, respectively) is negatively correlated with the $M_{R,bulk}$ (Figure S7). In general, f_{44}/f_{43} increases with altitude. There is an exception for two FT-BBA plumes with high $M_{R,bulk}$, but these coating thicknesses were also correlated with high f_{44}/f_{43}. Two hypotheses could explain the tendency of decreasing f_{44}/f_{43} ratio with increasing coating thickness: (i) the condensation of less-oxidized material onto preexisting highly aged organics favored by the lower temperature in the FT and/or (ii) fragmentation of highly oxidized organics induced by enhanced photochemical aging in the FT and subsequent evaporation (e.g., Ng et al., 2010; Palm et al., 2018). It should be noted here that the chemical composition was measured for bulk aerosols. It cannot be ruled out that the bulk f_{44}/f_{43} ratio is a poor indicator of the composition of the coating material on individual rBC-containing particles. While the exact reason for the variability in $M_{R,bulk}$ remains unclear, our results strongly suggest that atmospheric aging alters rBC mixing state through processes that are dynamic- and altitude-dependent.

3.2. Exploring the Sensitivity of BBA Optical Properties to rBC Mixing State

In Figure 2a, a large absorption enhancement in both BL-BBA and FT-BBA is evident. E_{abs} values range between 1.4 and 2.1, which correspond to MAC_{rBC} values between 10.8 and 16.2 m^2 g^{-1}. Our measured E_{abs} in BL-BBA is larger than the value of 1.5 commonly adopted in climate models when internal mixing of rBC is accounted for (Bond et al., 2013; Chung et al., 2012; Myhre, Samset, et al., 2013). The observed increase of E_{abs} with increasing $M_{R,bulk}$ indicates that a lensing-driven absorption enhancement is substantial in BBA. In field observations, significant absorption and strong spectral dependence (values of AAE >1.7) in BBA have frequently been attributed to the presence of BrC (Chakrabarty et al., 2010; Kirchstetter et al., 2004; Pokhrel et al., 2016; Romonosky et al., 2019; Sandradewi et al., 2008). Our measurements suggest that the contribution of BrC to light absorption is negligible, since
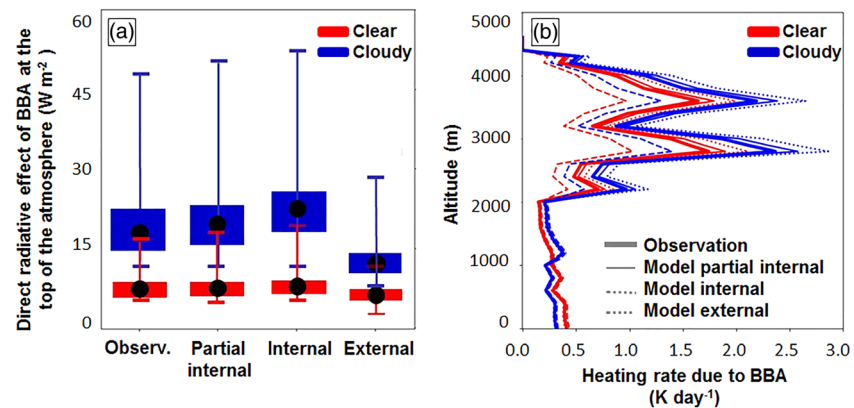
Figure 3. (a) Direct radiative effect (DRE) at the top of the atmosphere and (b) heating rate profile due to the transport of both BL-BBA and FT-BBA, calculated from measured and modeled BBA optical properties assuming different representation of rBC mixing state. On the left, the boxes mark the respective median values (middle points), the 25th and 75th percentiles (left and right box edges), and the minimum and maximum values (error bars). On the right, heating rate profiles are averaged over the campaign.

AAE values range from 0.8 to 1.1 (Figure 2b). These results imply that BBA absorption properties were largely dominated by the rBC mixing state. Figures 2c and 2d show decreases (increases) in the *SSA* (g) of the overall BBA population as f_{rBC} increases. When the air mass was transported in the FT, the *SSA* reached very low values (down to ~0.71), and rBC-containing particles contributed to the largest aerosol mass fraction (~18%). Despite this general trend, a large spread in *SSA* and g is observed independent of f_{rBC}.

To further investigate the variability on the observed optical properties, the core-shell Mie model was used to calculate E_{abs}, *SSA*, and g using the observed f_{rBC}, $D_{core\ rBC}$, and $D_{total\ rBC}$ and by assuming different rBC population mixing state. In the external mixing case, rBC-containing particles were assumed to be entirely uncoated, whereas the coating material is equally distributed across the population of rBC-containing particles in the internal mixing case. In the partial internal mixing case, the diversity in rBC mixing state is accounted for by combining internal and external configurations, parameterized using a simplified function of the observed $M_{R,bulk}$ (Figure S8). When an external mixing is considered, we find that E_{abs} and *SSA* are on average underestimated by ~42% and ~9.8% compared to observations (Figures 2a and 2c, respectively) and g overestimated by ~11% (Figure 2d). The fully rBC internal mixing assumption overestimates E_{abs} and *SSA* by ~13% and ~5.2%, respectively, and reduces the g bias to ~3.6%. When both mixing states coexist with the partial internal mixing case, the E_{abs} and *SSA* biases are reduced to ~5.1% and ~2.0%, respectively, which are in the range covered by the measurements uncertainties (i.e., 12% and 9%, respectively). This points out that accounting for the diversity of rBC mixing state is essential to properly model aerosol optical properties and that combining external and internal mixtures leads to more representative optical properties of BBA.

4. Implications for Atmospheric Radiation

Assuming that BBA absorption comes exclusively from spherical rBC-containing particles, the Mie scattering model successfully reproduces the observed BBA optical properties. Along with low *AAE* values, this suggests that BrC makes a negligible contribution to BBA optical properties at mid-visible wavelengths for well-aged air masses (larger than 1 week) that have undergone extensive oxidation. A plausible explanation is that BrC is removed during transport through photobleaching, volatilization, and/or cloud-phase reactions (Clarke et al., 2007; Forrister et al., 2015; Lewis et al., 2008), which leads to a higher fraction of rBC-containing particles in the total aerosol mass, lower *AAE*, and lower *SSA* values.

Our findings indicate that the treatment of rBC mixing state plays a significant role in resolving the BBA optical properties over the SWA region. To estimate the radiative importance of resolving the diversity of rBC mixing state in BBA plumes, radiative fluxes were computed with the radiative transfer model ecRad. In Figure 3, we examine the SW DRE at TOA and heating rates in clear-sky and cloudy-sky conditions

caused by BBA over SWA using measured and modeled BBA optical properties. BBA induces an intense positive SW DRE at TOA over the continental SWA in all-sky conditions, with the highest magnitude of the instantaneous forcing reaching +49 W m^{-2} for the more intense FT-BBA event. A sensitivity test of DRE to surface albedo suggests that, with a surface albedo of 0.1 closer to that of the ocean, BBA is able to exert either a positive or negative SW DRE at TOA depending on the presence of clouds (Figure S9), which is consistent with a large body of literature focused on this region (De Graaf et al., 2014; Feng & Christopher, 2015; Mallet et al., 2019; Meyer et al., 2013; Zuidema et al., 2016). In addition, the FT-BBA plumes lead to an ∼2.4 K d^{-1} increase in the average instantaneous SW heating rate in cloudy conditions, which can reach ∼6.0 K d^{-1} during extreme cases (Table S2). This increase in SW heating can reduce local relative humidity, implying a negative SDE over the ocean where absorbing BBA layers frequently exist above persistent stratus cloud decks (Ajoku et al., 2020; Herbert et al., 2020; Wilcox, 2012). In addition, the significant radiative impact of BBA highlighted in this study could also have some large implications on the stratus-to-cumulus cloud transition as shown by Deetz et al. (2018) during DACCIWA. Using unrealistic mixing state assumption for rBC-containing particles leads to notable systematic biases in the resulting DRE (heating rates) of ∼−26% (∼−40%) for externally and ∼+11% (∼−21%) for internally mixing, arising from underestimation and overestimation of the rBC absorption enhancement by the coating, respectively (Figures 3a and 3b). The range of extreme DRE values doubles from ∼ 4.5 (11) W m^{-2} in the external mixing case to ∼7.5 (22) W m^{-2} in the internal mixing case in clear-sky (cloudy) conditions (Figure 3a), reflecting the high sensitivity of BBA DRE to rBC coating thickness. The DRE and heating rates of BBA were successfully reproduced when the diversity of rBC mixing state is accounted for, which is currently unaccounted for in climate models (Chung et al., 2012; Mallet et al., 2019; Myhre, Samset, et al., 2013). Missing or incorrect representation of the internal rBC mixing state can thus contribute to a large underestimation or overestimation of BBA DRE and SW heating rates calculated by climate models in this region, depending on the mixing state assumption used.

5. Concluding Remarks

Using state-of-the-art airborne in situ measurements in conjunction with Mie scattering simulations, we demonstrate that the low *SSA* in BBA plumes over SWA results from the presence of strongly absorbing rBC-containing particles, whereas the BrC contribution to the BBA absorption is negligible. To date, climate models have been unsuccessful in reproducing the *SSA* in BBA plumes over eastern Atlantic Ocean (Lacagnina et al., 2015; Mallet et al., 2019; Peers et al., 2016; Stier et al., 2013). Our results show that accounting for the complex rBC mixing-state diversity (fraction of coated and uncoated rBC-containing particle and amount of scattering material on the rBC-containing particles) is needed to accurately estimate BBA optical properties. The assumed mixing state of rBC-containing particles controls the magnitude of the *SSA* and henceforth the SW DRE at TOA and heating rate of BBA. In addition, our results advise against the use of fixed timescales to represent aging of rBC-containing particles, as $M_{R,bulk}$ has been shown to vary with the altitude of BBA plumes, thus depending on local environmental conditions. Even though computational resources do not permit explicit calculation of aging by condensation and coagulation, some climate models have been moving towards aerosol modules that represent aerosol aging using several interacting modes (Aquila et al., 2011; Bauer et al., 2008; Fierce et al., 2016, 2017; Matsui et al., 2013; Stevens & Dastoor, 2019; Wilson et al., 2001). Accounting for a more realistic representation of rBC mixing state should significantly decrease the ambiguity in the radiative and climatic effects of BBA. Further studies testing the sensitivity of regional and global climate models to rBC mixing state representation are needed. Our measurements of rBC mixing state and vertically resolved abundances are broadly applicable to BBA over SWA for improvement in radiative transfer calculations, which would be very helpful to capture the full picture of how BBA modifies the atmospheric energy budget and cloud properties over SWA.

Data Availability Statement

All data used in this study are publicly available on the AERIS Data and Service Center, which can be found online (http://baobab.sedoo.fr/DACCIWA). Information on how to obtain ecRad for noncommercial education or research is available at the ecRad website (https://confluence.ecmwf.int/display/ECRAD).

References

Adebiyi, A. A., & Zuidema, P. (2016). The role of the southern African easterly jet in modifying the southeast Atlantic aerosol and cloud environments. *Quarterly Journal of the Royal Meteorological Society*, *142*(697), 1574–1589. https://doi.org/10.1002/qj.2765

Ajoku, O., Norris, J. R., & Miller, A. J. (2020). Observed monsoon precipitation suppression caused by anomalous interhemispheric aerosol transport. *Climate Dynamics*, *54*, 1077–1091. https://doi.org/10.1007/s00382-019-05046-y

Andreae, M. O., & Merlet, P. (2001). Emission of trace gases and aerosols from biomass burning. *Global Biogeochemical Cycles*, *15*(4), 955–966. https://doi.org/10.1029/2000GB001382

Aquila, V., Hendricks, J., Lauer, A., Riemer, N., Vogel, H., Baumgardner, D., et al. (2011). MADE-in: A new aerosol microphysics submodel for global simulation of insoluble particles and their mixing state. *Geoscientific Model Development*, *4*(2), 325–355. https://doi.org/10.5194/gmd-4-325-2011

Bauer, S. E., Wright, D. L., Koch, D., Lewis, E. R., Mc-Graw, R., Chang, L.-S., et al. (2008). MATRIX (multiconfiguration aerosol TRacker of mIXing state): An aerosol microphysical module for global atmospheric models. *Atmospheric Chemistry and Physics*, *8*(20), 6003–6035. https://doi.org/10.5194/acp-8-6003-2008

Bohren, C. F., & Huffman, D. R. (1983). *Absorption and scattering of light by small particles*. New York: Wiley.

Bond, T. C., & Bergstrom, R. W. (2006). Light absorption by carbonaceous particles: An investigative review. *Aerosol Science and Technology*, *40*(1), 27–67. https://doi.org/10.1080/02786820500421521

Bond, T. C., Doherty, S. J., Fahey, D. W., Forster, P. M., Berntsen, T., DeAngelo, B. J., et al. (2013). Bounding the role of black carbon in the climate system: 755 A scientific assessment. *Journal of Geophysical Research: Atmospheres*, *118*, 5380–5552. https://doi.org/10.1002/jgrd.50171

Bond, T. C., Streets, D. G., Yarber, K. F., Nelson, S. M., Woo, J.-H., & Klimont, Z. (2004). A technology-based global inventory of black and organic carbon emissions from combustion. *Journal of Geophysical Research*, *109*, D14203. https://doi.org/10.1029/2003JD003697

Brito, J., Freney, E., Dominutti, P., Borbon, A., Haslett, S. L., Batenburg, A. M., et al. (2018). Assessing the role of anthropogenic and biogenic sources on PM1 over southern West Africa using aircraft measurements. *Atmospheric Chemistry and Physics*, *18*, 757–772. https://doi.org/10.5194/acp-18-757-2018

Brown, H., Liu, X., Feng, Y., Jiang, Y., Wu, M., Lu, Z., et al. (2018). Radiative effect and climate impacts of brown carbon with the Community Atmosphere Model (CAM5). *Atmospheric Chemistry and Physics*, *18*, 17,745–17,768. https://doi.org/10.5194/acp-18-17745-2018

Capes, G., Johnson, B., McFiggans, G., Williams, P. I., Haywood, J. M., & Coe, H. (2008). Aging of biomass burning aerosols over West Africa: Aircraft measurements of chemical composition, microphysical properties and emission ratios. *Journal of Geophysical Research*, *113*, D00C15. https://doi.org/10.1029/2008JD009845

Cappa, C. D., Onasch, T. B., Massoli, P., Worsnop, D. R., Bates, T. S., Cross, E. S., et al. (2012). Radiative absorption enhancements due to the mixing state of atmospheric black carbon. *Science*, *337*, 1078–1081. https://doi.org/10.1126/science.1223447

Chakrabarty, R. K., Moosmüller, H., Chen, L.-W. A., Lewis, K., Arnott, W. P., Mazzoleni, C., et al. (2010). Brown carbon in tar balls from smoldering biomass combustion. *Atmospheric Chemistry and Physics*, *10*(13), 6363–6370. https://doi.org/10.5194/acp-10-6363-2010

Chung, C. E., Ramanathan, V., & Decremer, D. (2012). Observationally constrained estimates of carbonaceous aerosol radiative forcing. *Proceedings of the National Academy of Sciences*, *109*(29), 11,624–11,629. https://doi.org/10.1073/pnas.1203707109

Chylek, P., Lee, J. E., Romonosky, D. E., Gallo, F., Lou, S., Shrivastava, M., et al. (2019). Mie scattering captures observed optical properties of ambient biomass burning plumes assuming uniform black, brown, and organic carbon mixtures. *Journal of Geophysical Research: Atmospheres*, *124*, 11,406–11,427. https://doi.org/10.1029/2019JD031224

Clarke, A., McNaughton, C., Kapustin, V., Shinozuka, Y., Howell, S., Dibb, J., et al. (2007). Biomass burning and pollution aerosol over North America: Organic components and their influence on spectral optical properties and humidification response. *Journal of Geophysical Research*, *112*, D12S18. https://doi.org/10.1029/2006JD007777

Davies, N. W., Fox, C., Szpek, K., Cotterell, M. I., Taylor, J. W., Allan, J. D., et al. (2019). Evaluating biases in filter-based aerosol absorption measurements using photoacoustic spectroscopy. *Atmospheric Measurement Techniques*, *12*, 3417–3434. https://doi.org/10.5194/amt-12-3417-2019

De Graaf, M., Bellouin, N., Tilstra, L. G., Haywood, J., & Stammes, P. (2014). Aerosol direct radiative effect of smoke over clouds over the southeast Atlantic Ocean from 2006 to 2009. *Geophysical Research Letters*, *41*, 7723–7730. https://doi.org/10.1002/2014GL061103

Deetz, K., Vogel, H., Knippertz, P., Adler, B., Taylor, J., Coe, H., et al. (2018). Numerical simulations of aerosol radiative effects and their impact on clouds and atmospheric dynamics over southern West Africa. *Atmospheric Chemistry and Physics*, *18*, 9767–9788. https://doi.org/10.5194/acp-18-9767-2018

Denjean, C., Bourrianne, T., Burnet, F., Mallet, M., Maury, N., Colomb, A., et al. (2020). Overview of aerosol optical properties over southern West Africa from DACCIWA aircraft measurements. *Atmospheric Chemistry and Physics*, *20*, 4735–4756. https://doi.org/10.5194/acp-20-4735-2020

Denjean, C., Cassola, F., Mazzino, A., Triquet, S., Chevaillier, S., Grand, N., et al. (2016). Size distribution and optical properties of mineral dust aerosols transported in the western Mediterranean. *Atmospheric Chemistry and Physics*, *16*, 1081–1104. https://doi.org/10.5194/acp-16-1081-2016

Edwards, J. M., & Slingo, A. (1996). Studies with a flexible new radiation code: 1. Choosing a configuration for a large-scale model. *Quarterly Journal of the Royal Meteorological Society*, *122*(531), 689–719. https://doi.org/10.1002/qj.49712253107

Feng, N., & Christopher, S. A. (2015). Measurement-based estimates of direct radiative effects of absorbing aerosols above clouds. *Journal of Geophysical Research: Atmospheres*, *120*, 6908–6921. https://doi.org/10.1002/2015JD023252

Fierce, L., Bond, T. C., Bauer, S. E., Mena, F., & Riemer, N. (2016). Black carbon absorption at the global scale is affected by particle-scale diversity in composition. *Nature Communications*, *7*, 12361. https://doi.org/10.1038/ncomms12361

Fierce, L., Riemer, N., & Bond, T. C. (2017). Toward reduced representation of mixing state for simulating aerosol effects on climate. *Bulletin of the American Meteorological Society*, *98*(5), 971–980. https://doi.org/10.1175/bams-d-16-0028.1

Flamant, C., Deroubaix, A., Chazette, P., Brito, J., Gaetani, M., Knippertz, P., et al. (2018). Aerosol distribution in the northern Gulf of Guinea: Local anthropogenic sources, long-range transport, and the role of coastal shallow circulations. *Atmospheric Chemistry and Physics*, *18*, 12,363–12,389. https://doi.org/10.5194/acp-18-12363-2018

Flamant, C., Knippertz, P., Fink, A. H., Akpo, A., Brooks, B., Chiu, C. J., et al. (2018). The dynamics-aerosol-chemistry-cloud interactions in West Africa field campaign: Overview and research highlights. *Bulletin of the American Meteorological Society*, *99*, 83–104. https://doi.org/10.1175/BAMS-D-16-0256.1

Formenti, P., D'Anna, B., Flamant, C., Mallet, M., Piketh, S. J., Schepanski, K., et al. (2019). The aerosols, radiation and clouds in southern Africa (AEROCLO-sA) field campaign in Namibia: Overview, illustrative observations and way forward. *Bulletin of the American Meteorological Society*, *100*, 1277–1298. https://doi.org/10.1175/BAMS-D-17-0278.1

Forrister, H., Liu, J., Scheuer, E., Dibb, J., Ziemba, L., Thornhill, K. L., et al. (2015). Evolution of brown carbon in wildfire plumes. *Geophysical Research Letters*, *42*, 4623–4630. https://doi.org/10.1002/2015GL063897

Fuller, K. A., Malm, W. C., & Kreidenweis, S. M. (1999). Effects of mixing on extinction by carbonaceous particles. *Journal of Geophysical Research*, *104*(D13), 15,941–15,954. https://doi.org/10.1029/1998JD100069

Gao, R. S., Schwarz, J. P., Kelly, K. K., Fahey, D. W., Watts, L. A., Thompson, T. L., et al. (2007). A novel method for estimating light-scattering properties of soot aerosols using a modified single-particle soot photometer. *Aerosol Science and Technology*, *41*(2), 125–135. https://doi.org/10.1080/02786820601118398

Haslett, S. L., Taylor, J. W., Evans, M., Morris, E., Vogel, B., Dajuma, A., et al. (2019). Remote biomass burning dominates southern West African air pollution during the monsoon. *Atmospheric Chemistry and Physics*, *19*, 15,217–15,234. https://doi.org/10.5194/acp-19-15217-2019

Healy, R. M., Wang, J. M., Jeong, C. H., Lee, A. K. Y., Willis, M. D., Jaroudi, E., et al. (2015). Light-absorbing properties of ambient black carbon and brown carbon from fossil fuel and biomass burning sources. *Journal of Geophysical Research: Atmospheres*, *120*, 6619–6633. https://doi.org/10.1002/2015JD023382

Herbert, R. J., Bellouin, N., Highwood, E. J., & Hill, A. A. (2020). Diurnal cycle of the semi-direct effect from a persistent absorbing aerosol layer over marine stratocumulus in large-eddy simulations. *Atmospheric Chemistry and Physics*, *20*, 1317–1340. https://doi.org/10.5194/acp-20-1317-2020

Hogan, R. J., & Bozzo, A. (2018). A flexible and efficient radiation scheme for the ECMWF model. *Journal of Advances in Modeling Earth Systems*, *10*, 1990–2008. https://doi.org/10.1029/2018MS001364

Kahnert, M., & Kanngießer, F. (2020). Modelling optical properties of atmospheric black carbon aerosols. *Journal of Quantitative Spectroscopy and Radiative Transfer*, *244*, 106849. https://doi.org/10.1016/j.jqsrt.2020.106849

Kirchstetter, T. W., Novakov, T., & Hobbs, P. (2004). Evidence that the spectral dependence of light absorption by aerosols is affected by organic carbon. *Journal of Geophysical Research*, *109*, D21208. https://doi.org/10.1029/2004JD004999

Knippertz, P., Coe, H., Chiu, J. C., Evans, M. J., Fink, A. H., Kalthoff, N., et al. (2015). The DACCIWA project: Dynamics-aerosol-chemistry-cloud interactions in West Africa. *Bulletin of the American Meteorological Society*, *96*, 1451–1460. https://doi.org/10.1175/BAMS-D-14-00108.1, http://journals.ametsoc.org/

Laborde, M., Mertes, P., Zieger, P., Dommen, J., Baltensperger, U., & Gysel, M. (2012). Sensitivity of the Single Particle Soot Photometer to different black carbon types. *Atmospheric Measurement Techniques*, *5*, 1031–1043. https://doi.org/10.5194/amt-5-1031-2012

Lacagnina, C., Hasekamp, O. P., Bian, H., Curci, G., Myhre, G., van Noije, T., et al. (2015). Aerosol single-scattering albedo over the global oceans: Comparing PARASOL retrievals with AERONET, OMI, and AeroCom models estimates. *Journal of Geophysical Research: Atmospheres*, *120*, 9814–9836. https://doi.org/10.1002/2015JD023501

Lack, D. A., Langridge, J. M., Bahreini, R., Cappa, C. D., Middlebrook, A. M., & Schwarz, J. P. (2012). Brown carbon and internal mixing in biomass burning particles. *Proceedings. National Academy of Sciences. United States of America*, *109*(37), 14,802–14,807. https://doi.org/10.1073/pnas.1206575109

Lewis, K., Arnott, W. P., Moosmuller, H., & Wold, C. E. (2008). Strong spectral variation of biomass smoke light absorption and single scattering albedo observed with a novel dual-wavelength photoacoustic instrument. *Journal of Geophysical Research*, *113*, D16203. https://doi.org/10.1029/2007JD009699

Liu, D., Whitehead, J., Alfarra, M. R., Reyes-Villegas, E., Spracklen, D. V., Reddington, C. L., et al. (2017). Black-carbon absorption enhancement in the atmosphere determined by particle mixing state. *Nature Geoscience*, *10*, 184–188. https://doi.org/10.1038/ngeo2901

Liu, L., & Mishchenko, M. I. (2007). Scattering and radiative properties of complex soot and soot-containing aggregate particles. *Journal of Quantitative Spectroscopy & Radiative Transfer*, *106*, 262–273. https://doi.org/10.1016/j.jqsrt.2007.01.020

Mallet, M., Nabat, P., Zuidema, P., Redemann, J., Sayer, A. M., Stengel, M., et al. (2019). Simulation of the transport, vertical distribution, optical properties and radiative impact of smoke aerosols with the ALADIN regional climate model during the ORACLES-2016 and LASIC experiments. *Atmospheric Chemistry and Physics*, *19*, 4963–4990. https://doi.org/10.5194/acp-19-4963-2019

Matsui, H., Koike, M., Kondo, Y., Moteki, N., Fast, J. D., & Zaveri, R. A. (2013). Development and validation of a black carbon mixing state resolved three-dimensional model: Aging processes and radiative impact. *Journal of Geophysical Research: Atmospheres*, *118*, 2304–2326. https://doi.org/10.1029/2012JD018446

Menut, L., Flamant, C., Turquety, S., Deroubaix, A., Chazette, P., & Meynadier, R. (2018). Impact of biomass burning on pollutant surface concentrations in megacities of the Gulf of Guinea. *Atmospheric Chemistry and Physics*, *18*, 2687–2707. https://doi.org/10.5194/acp-18-2687-2018

Meyer, K., Platnick, S., Oreopoulos, L., & Lee, D. (2013). Estimating the direct radiative effect of absorbing aerosols overlying marine boundary layer clouds in the southeast Atlantic using MODIS and CALIOP. *Journal of Geophysical Research: Atmospheres*, *118*, 4801–4815. https://doi.org/10.1002/jgrd.50449

Moody, E. G., King, M. D., Platnick, S., Schaaf, C. B., & Gao, F. (2005). Spatially complete global spectral surface albedos: Value-added datasets derived from Terra MODIS land products. *IEEE Transactions on Geoscience and Remote Sensing*, *43*(1), 144–158. https://doi.org/10.1109/TGRS.2004.838359

Moteki, N., Kondo, Y., Oshima, N., Takegawa, N., Koike, M., Kita, K., et al. (2012). Size dependence of wet removal of black carbon aerosols during transport from the boundary layer to the free troposphere. *Geophysical Research Letters*, *39*, L13802. https://doi.org/10.1029/2012GL052034

Muller, T., Laborde, M., Kassell, G., & Wiedensohler, A. (2011). Design and performance of a three-wavelength LED-based total scatter and backscatter integrating nephelometer. *Atmospheric Measurement Techniques*, *4*, 1291–1303. https://doi.org/10.5194/amt-4-1291-2011

Myhre, G., Samset, B. H., Schulz, M., Balkanski, Y., Bauer, S., Berntsen, T. K., et al. (2013). Radiative forcing of the direct aerosol effect from AeroCom Phase II simulations. *Atmospheric Chemistry and Physics*, *13*, 1853–1877. https://doi.org/10.5194/acp-13-1853-2013

Myhre, G., Shindell, D., Bréon, F.-M., Collins, W., Fuglestvedt, J., Huang, J., et al. (2013). Anthropogenic and natural radiative forcing. In T. F. Stocker, D. Qin, G.-K. Plattner, M. Tignor, S. K. Allen, J. Boschung, A. Nauels, Y. Xia, V. Bex, & P. M. Midgley (Eds.), *Climate Change 2013: The Physical Science Basis, Contribution of Working Group I to the Fifth Assessment Report of the Intergovernmental Panel on Climate Change* (pp. 659–740). Cambridge, UK and New York, NY, USA: Cambridge University Press.

Ng, N. L., Canagaratna, M. R., Zhang, Q., Jimenez, J. L., Tian, J., Ulbrich, I. M., et al. (2010). Organic aerosol components observed in Northern Hemispheric datasets from aerosol mass spectrometry. *Atmospheric Chemistry and Physics*, *10*(10), 4625–4641. https://doi.org/10.5194/acp-10-4625-2010

Palm, B. B., de Sá, S. S., Day, D. A., Campuzano-Jost, P., Hu, W., Seco, R., et al. (2018). Secondary organic aerosol formation from ambient air in an oxidation flow reactor in central Amazonia. *Atmospheric Chemistry and Physics*, *18*, 467–493. https://doi.org/10.5194/acp-18-467-2018

Peers, F., Bellouin, N., Waquet, F., Ducos, F., Goloub, P., Mollard, J., et al. (2016). Comparison of aerosol optical properties above clouds between POLDER and AeroCom models over the South East Atlantic Ocean during the fire season. *Geophysical Research Letters*, *43*, 3991–4000. https://doi.org/10.1002/2016GL068222

Pistone, K., Redemann, J., Doherty, S., Zuidema, P., Burton, S., Cairns, B., et al. (2019). Intercomparison of biomass burning aerosol optical properties from in situ and remote-sensing instruments in ORACLES-2016. *Atmospheric Chemistry and Physics*, *19*, 9181–9208. https://doi.org/10.5194/acp-19-9181-2019

Pokhrel, R. P., Wagner, N. L., Langridge, J. M., Lack, D. A., Jayarathne, T., Stone, E. A., et al. (2016). Parameterization of single-scattering 1060 albedo (SSA) andabsorption Ångström exponent (AAE) with EC/OC for aerosol emissions 1061 from biomass burning. *Atmospheric Chemistry and Physics*, *16*, 9549–9561. https://doi.org/10.5194/acp-16-10629549-2016

Randles, C. A., & Ramaswamy, V. (2010). Direct and semi-direct impacts of absorbing biomass burning aerosol on the climate of southern Africa: A Geophysical Fluid Dynamics Laboratory GCM sensitivity. *Atmospheric Chemistry and Physics*, *10*(20), 9819–9831. https://doi.org/10.5194/acp-10-9819-2010

Romonosky, D., Gomez, S., Lam, J., Carrico, C., Aiken, A., Chylek, P., & Dubey, M. (2019). Optical properties of Laboratory & Ambient Biomass Burning Aerosols: Elucidating black, Brown, & organic carbon components & mixing regimes. *Journal of Geophysical Research: Atmospheres*, *124*, 5088–5105. https://doi.org/10.1029/2018JD029892

Sakaeda, N., Wood, R., & Rasch, P. J. (2011). Direct and semidirect aerosol effects of southern African biomass burning aerosol. *Journal of Geophysical Research*, *116*, D12205. https://doi.org/10.1029/2010JD015540

Sandradewi, J., Prevot, A. S. H., Weingartner, E., Schmidhauser, R., Gysel, M., & Baltensperger, U. (2008). A study of wood burning and traffic aerosols in an Alpine valley using a multi-wavelength Aethalometer. *Atmospheric Environment*, *42*(1), 101–112. https://doi.org/10.1016/j.atmosenv.2007.09.034

Shingler, T., Sorooshian, A., Ortega, A., Crosbie, E., Wonaschütz, A., Perring, A. E., et al. (2016). Ambient observations of hygroscopic growth factor and *f* (RH) below 1: Case studies from surface and airborne measurements. *Journal of Geophysical Research: Atmospheres*, *121*, 13,661–13,677. https://doi.org/10.1002/2016JD025471

Spackman, J. R., Schwarz, J. P., Gao, R. S., Watts, L. A., Thomson, D. S., Fahey, D. W., et al. (2008). Empirical correlations between black carbon aerosol and carbon monoxide in the lower and middle troposphere. *Geophysical Research Letters*, *35*, L19816. https://doi.org/10.1029/2008gl035237

Stevens, R., & Dastoor, A. (2019). A review of the representation of aerosol mixing state in atmospheric models. *Atmosphere*, *10*, 168. https://doi.org/10.3390/atmos10040168

Stier, P., Schutgens, N. A. J., Bellouin, N., Bian, H., Boucher, O., Chin, M., et al. (2013). Host model uncertainties in aerosol radiative forcing estimates: Results from the AeroCom Prescribed intercomparison study. *Atmospheric Chemistry and Physics*, *13*, 3245–3270. https://doi.org/10.5194/acp-13-3245-2013

Taylor, J. W., Allan, J. D., Allen, G., Coe, H., Williams, P. I., Flynn, M. J., et al. (2014). Size-dependent wet removal of black carbon in Canadian biomass burning plumes. *Atmospheric Chemistry and Physics*, *14*, 13,755–13,771. https://doi.org/10.5194/acp-14-13755-2014

Taylor, J. W., Haslett, S. L., Bower, K., Flynn, M., Crawford, I., Dorsey, J., et al. (2019). Aerosol influences on low-level clouds in the West African monsoon. *Atmospheric Chemistry and Physics*, *19*, 8503–8522. https://doi.org/10.5194/acp-19-8503-2019

Virkkula, A. (2010). Correction of the calibration of the 3-wavelength Particle Soot Absorption Photometer (3λ PSAP). *Aerosol Science and Technology*, *44*(8), 706–712. https://doi.org/10.1080/02786826.2010.482110

Waquet, F., Peers, F., Ducos, F., Goloub, P., Platnick, S., Riedi, J., et al. (2013). Global analysis of aerosol properties above clouds. *Geophysical Research Letters*, *40*, 5809–5814. https://doi.org/10.1002/2013GL057482

Wilcox, E. M. (2010). Stratocumulus cloud thickening beneath layers of absorbing smoke aerosol. *Atmospheric Chemistry and Physics*, *10*, 11,769–11,777. https://doi.org/10.5194/acp-10-11769-2010

Wilcox, E. M. (2012). Direct and semi-direct radiative forcing of smoke aerosols over clouds. *Atmospheric Chemistry and Physics*, *12*, 139–149. https://doi.org/10.5194/acp-12-139-2012

Wilson, J., Cuvelier, C., & Raes, F. (2001). A modeling study of global mixed aerosol fields. *Journal of Geophysical Research*, *106*(D24), 34,081–34,108. https://doi.org/10.1029/2000JD000198

Wu, H., Taylor, J. W., Szpek, K., Langridge, J., Williams, P. I., Flynn, M., et al. (2020). Vertical variability of the properties of highly aged biomass burning aerosol transported over the southeast Atlantic during CLARIFY-2017. *Atmospheric Chemistry and Physics Discussions*. https://doi.org/10.5194/acp-2020-197, in review

Wu, Y., Cheng, T., Liu, D., Allan, J. D., Zheng, L., & Chen, H. (2018). Light absorption enhancement of black carbon aerosol constrained by particle morphology. *Environmental Science & Technology*, *52*(12), 6912–6919. https://doi.org/10.1021/acs.est.8b00636

Zuidema, P., Redemann, J., Haywood, J., Wood, R., Piketh, S., Hipondoka, M., & Formenti, P. (2016). Smoke and clouds above the southeast Atlantic: Upcoming field campaigns probe absorbing aerosols impact on climate. *Bulletin of the American Meteorological Society*, *97*, 1131–1135. https://doi.org/10.1175/BAMS-D-15-00082.1

Zuidema, P., Sedlacek, A. J. III, Flynn, C., Springston, S., Delgadillo, R., Zhang, J., et al. (2018). The Ascension Island boundary layer in the remote southeast Atlantic is often smoky. *Geophysical Research Letters*, *45*, 4456–4465. https://doi.org/10.1002/2017GL076926